Linear Dipole Behavior in Single CdSe-Oligo(phenylene vinylene) Nanostructures

K. T. Early,[†] K. D. McCarthy,[†] M. Y. Odoi,[†] P. K. Sudeep,[‡] T. Emrick,[‡] and M. D. Barnes[†,*]

[†]George R. Richason Jr. Chemistry Laboratory, Department of Chemistry, University of Massachusetts Amherst, Amherst, Massachusetts 01003, and [‡]Department of Polymer Science and Engineering, University of Massachusetts Amherst, Amherst, Massachusetts 01003

ARTICLE

ABSTRACT We report on linearly polarized absorption and emission from individual (4.3 nm) CdSe quantum dots whose surfaces are coordinated with monodisperse oligo-phenylene vinylene ligands. Shown previously to suppress quantum dot blinking, we demonstrate here that the electronic interaction of photoexcited ligands with the quantum dot core is manifested as a strong polarization anisotropy in absorption ($M = 0.5$), as well as distinct linear dipole emission patterns from the quantum dot core. Further, there is a correlation between the quantum dot emission moment and polarization orientation corresponding to the absorption maxima that is manifested as fluctuations in emission moment orientation in the $X-Y$ plane. The observed polarization effects can be switched off by tuning the excitation away from the ligand absorption band. We propose a mechanism based on exciton dissociation from the photoexcited ligand, followed by the pinning of electrons at the quantum dot surface. The resulting Stark interaction is sufficiently strong to break the 2D degeneracy of the emission moment within the dot, and may therefore account for the linear dipole emission character.

KEYWORDS: CdSe quantum dots · dipole transitions · ligand effects · surface charges · defocused imaging · polarization anisotropy

Hybrid organic/inorganic materials have been investigated extensively as active layers in photovoltaic materials.[1,2] Devices based on blends of semiconductor quantum dots (QDs) and conjugated semiconductor polymers are attractive for several reasons. The broadband optical absorption and tunable band gap in CdSe QDs makes them ideal sensitizers for hybrid photovoltaics; conjugated polymers, with their high charge mobility[3] and adaptable morphologies, provide efficient scaffolds. However, significant problems are encountered in quantum dot−polymer blends. Engineering nanoscale domains of the scale of exciton diffusion lengths remains a great challenge, resulting in capacitance effects and radiative recombination. Even assuming intimate polymer−nanocrystal contact, structural disorder and heterogeneity in films leads to ill-defined dipole transitions in the polymer and nanocrystal components, inhibiting transfer of excitations between the two domains. As a result, efficient charge mobility in these devices occurs only at large nanocrystal loadings.[2,4] Understanding and controlling the interaction and energy/charge flow in both components is critical to improving performance in this class of materials.

Polarization properties, morphology-dependent photophysics, and energy and charge transport have been well studied in conjugated organic systems. Buratto, for example, has described interchromophore interactions in tetrapodal *versus* single oligomer phenylene vinylene systems.[5−7] Peteanu and co-workers have investigated the spectroscopy of size-selected molecular aggregates and shown how the photophysics depends on the chromophore alignment of the aggregated system.[8,9] Barbara has made extensive studies of the single-molecule spectroscopy of poly(phenylene vinylene) derivatives and made important contributions to understanding the connection between molecular morphology and single-molecule photophysics.[10] Lupton and co-workers have made important contributions to the study of chromophore−chromophore interactions in conjugated polymers, providing insight into mechanisms for energy and charge migration in complex molecular structures.[11−14] Polarization anisotropy studies on single organic chromophores by Ha *et al.*[15] and Macklin *et al.*[16] provide insight into the transition moments and dynamics with high resolution, confirming the polarization of the electric dipole transition along the conjugation axis of these chromophores. Our own research has focused on effects of nanoscale confinement on single-molecules of conjugated polymers using modified ink-jet printing techniques. We showed that oriented nanostructures form readily by confining single MEH-PPV molecules to subpicoliter liquid

*Address correspondence to mdbarnes@chem.umass.edu.

Received for review November 19, 2008 and accepted January 20, 2009.

Published online February 3, 2009.
10.1021/nn800785s CCC: $40.75

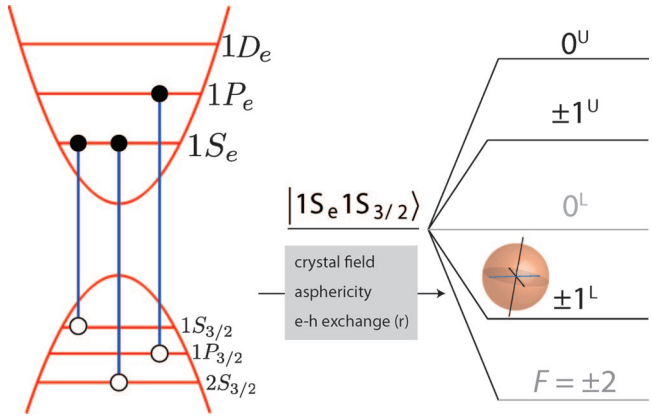

Figure 1. (Left) State diagram of the lowest energy transitions in a CdSe nanocrystal. The band-edge is the $1S_e-1S_{3/2}$ transition. (Right) Splitting of the $1S_e-1S_{3/2}$ transition arising from crystal field and exchange splitting, as well as shape defects. The lowest allowed transition, $F = \pm1^L$, is depicted as its two orthogonal, linearly polarized components in the equatorial disk.

droplets, where confinement and droplet evaporation drive collapse transitions to form nanostructures with a high degree of internal order and interesting photophysical properties.[17−20]

Unlike the strictly linearly polarized transitions in conjugated organic molecules described above, the band-edge transitions in colloidal QDs are, to a good first approximation, unpolarized in emission due both to intrinsic (electronic) as well as extrinsic (random orientation) effects. The nature of intrinsic electric dipole transitions in CdSe nanocrystals continues to be a topic of great interest. Detailed theoretical models[21,22] of wurtzite CdSe nanocrystals predict a manifold of transitions, of which the $|1^L\rangle$ is the lowest energy optically active transition. This $|1^L\rangle$ state is characterized by a transition moment "disk" orthogonal to the crystal axis and appears in most reports to be degenerate for spherical nanocrystals, thus often referred to as a 2D degenerate dipole. Deviations from this degenerate behavior so far have been limited to studies on asymmetric QDs at cryogenic[23] and ambient[24] temperatures and asymmetric CdSe structures (*i.e.*, nanorods),[25] largely because the energy splittings of the orthogonal components of the $|1^L\rangle$ transition are small (<3 meV). This difficulty in enforcing directionality in the transition moment of individual nanocrystals is a primary reason for the current focus on self-assembled QDs in optoelectronics and spintronics as opposed to individual or isolated quantum dots.

We recently reported enhanced spectral stability and suppressed fluorescence intermittency (blinking) in CdSe nanocrystals coordinated with paraphenylene vinylene oligomers (CdSe-OPV).[26] In these nanostructures the OPV ligands serve as a surface passivating layer on the quantum dots, and are spectrally positioned as energy donors in Forster excitation transfer to the nanocrystal acceptor. We speculated that the presence of the capping ligands, in which excitons are generated under continuous wave (cw) illumination, transfer charge carriers to the nanocrystal surface and passivate localized trap sites, thereby also reducing residence times in so-called "dark states" in photoluminescence. In this scheme, one would expect the polarization characteristics of the organic ligands to be superimposed on the QD in absorption. Here we show that, when excited in a wavelength region where both OPV and CdSe absorb, individual CdSe-OPV nanostructures display both strong linear dichroism *and* linearly polarized emission (manifested in dipole emission pattern imaging), in addition to the previously reported blinking suppression. By tuning the excitation closer to the CdSe band edge and away from the OPV absorption band, these effects are strongly suppressed. We propose a mechanism based on a directional Stark interaction caused by photoproduced excitons in the organic ligands that break the symmetry of the nanocrystal core. These results provide strong evidence of transfer of the linearly polarized transitions of OPV molecules to pseudospherical CdSe QDs, resulting in hybrid structures that display the polarization properties of conjugated organic molecules and the robust photoluminescence of nanocrystalline quantum dots.

BACKGROUND

Numerous theoretical[21,22] and experimental[27,28] studies on colloidal QDs have examined the character of the transition dipole moment in CdSe nanocrystals capped with passive surface ligands and/or a ZnS shell. The splitting of the band edge $1S_e-1S_{3/2}$ exciton in CdSe nanocrystals into a five-state manifold has been predicted by perturbation theory and verified experimentally[27,29] (see Figure 1, left). The so-called "bright exciton" $|1^L\rangle$ state with angular momentum $F = \pm1$ has been the focus of several recent experiments, in which the structure of the so-called 2D degenerate dipole moment of wurtzite nanocrystals has been verified. This circularly symmetric dipole moment can be represented as an equatorial disk about the minor axis of slightly prolate nanocrystals in the plane perpendicular to the crystalline *c*-axis. This transition dipole moment structure has been confirmed by polarization anisotropy measurements[30,31] as well as imaging of the defocused photon distribution patterns of single crystals,[32,33] which appear as the summed intensity of two orthogonal, independent emitters. These experiments have been used to rapidly determine the laboratory-frame orientation of the crystal *c*-axis of individual nanocrystals.

Recent low-temperature experiments by Klimov and co-workers[23] have uncovered a slight degeneracy breaking in asymmetric CdSe/ZnS nanocrystals. In these experiments, the $|1^L\rangle$ state is further resolved into linearly polarized, orthogonal sublevels

$$|X\rangle = (1/\sqrt{2})(|+1\rangle + |-1\rangle) \quad \text{and}$$

$$|Y\rangle = (1/\sqrt{2})(|+1\rangle - |-1\rangle)$$

These sublevels split the 2D degenerate dipole into mutually orthogonal components, resulting from small differences in the exciton exchange interaction at the elliptical equator,[23,27,33] shown schematically in Figure 1, right. These components were shown in approximately 10% of the nanocrystals sampled to have a nonzero energy splitting on the order of 1−2 meV, scaling with nanocrystal volume.

Until now, direct visualization of any splitting of this equatorial transition moment has been in the form of modified 2D transition dipoles[34,35] (i.e., 3 1D dipoles, 2D + 1D dipoles). Such modified transition moments likely arise from sample-to-sample heterogeneities, because the ratio of oscillator strengths between the $|1^L\rangle$ (degenerate) and $|0^{UL}\rangle$ (linear) transitions depends strongly on crystal shape.[22,27] In this report, we independently access the orthogonal components of the $|1^L\rangle$ transition at room temperature, which is manifested as a discontinuous jump between two emission moment orientations under rotating pump polarization in the $X-Y$ plane. The modifications to the nanocrystal electronic structure by the conjugated OPV oligomers, we believe, arise from asymmetrically Stark-modified $|X\rangle$ and $|Y\rangle$ QD states from charge separated ligands. In the case of a pinned charge at the surface of the nanocrystal, these shifts have been calculated to be on the order of 70−75 meV.

RESULTS

Linear Dichroism. Linear dichroism is a measure of the polarization response of a single molecule to a rotating excitation field and has been used extensively to examine the nature of the transition dipole moment in organic chromophores.[15,16,36] Conjugated organic molecules, which have transition moments polarized along the conjugation axis normally show very strong linear dichroism. These measurements can thus be used to determine the laboratory-frame orientation of the molecular absorption moment. The modulation depth, given here by $M = (I_{max} - I_{min})/(I_{max} + I_{min})$ where I_{max} (I_{min}) corresponds to the maximum (minimum) detector counts in a single polarization rotation, ranges from 0 to 1. Isotropic absorbers, such as dye-doped polystyrene beads containing hundreds of randomly oriented linear chromophores within a diffraction limited spot, exhibit a negligible modulation depth, while single linear absorbers such as DiI show near-unity modulation depths. Such polarization anisotropy experiments have also been carried out on CdSe/ZnS core−shell nanocrystals by Bawendi and co-workers,[30,31] showing a modulation depth centered around $M = 0.5$ for an ensemble of single nanocrystals dispersed in polymethylmethacrylate. This value was attributed to the large collection angle of the high-NA objective used, the intrinsic nanocrystal transition moments, and the modified dipole radiation patterns in the proximity of the dielectric (glass) surface.[31]

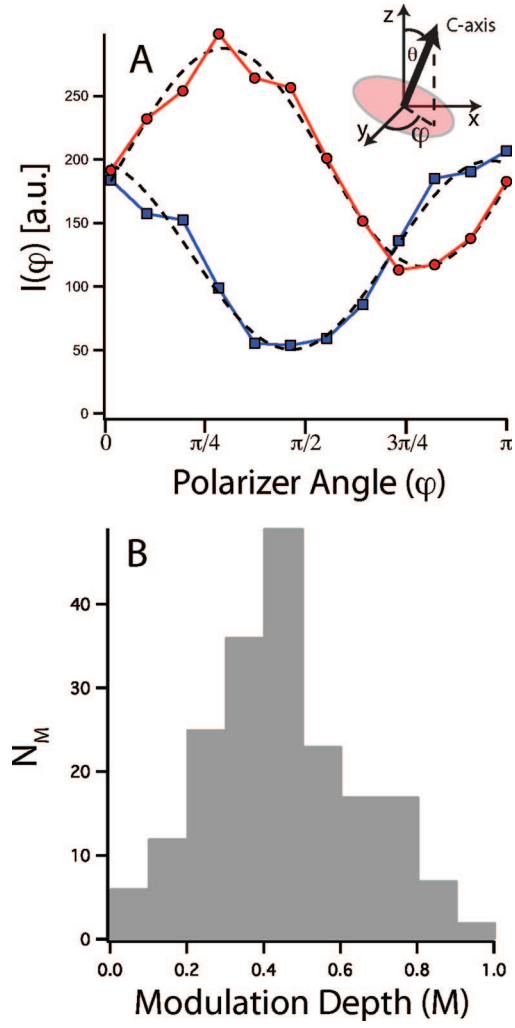

Figure 2. (A) Experimental polarization modulation traces for 2 CdSe-OPV nanostructures. The phase offset of 60° is real, showing no experimental polarization bias. The fitting parameters for each particle are $M = 0.58$, $\theta = 59°$ (●) and $M = 0.45$, $\theta = 52°$ (■). The dashed lines are fits to $\cos^2(\varphi)$ functions. Inset: Schematic representation of a 2D transition dipole moment with normal crystal *c*-axis at polar angle θ and azimuthal angle φ. (B) Histogram of *M* parameters for 200 CdSe-OPV nanostructures, with $\bar{M} = 0.47$.

In the 2D degenerate picture, the ellipse projected onto the sample plane determines the modulation depth for a single randomly dispersed QD, depicted schematically in the inset of Figure 2A. We denote the orientation of the nanocrystal by the polar coordinates (θ, φ) made by the crystal *c*-axis relative to the *z* (optic) axis of the experiment. The intensity of excitation (and therefore emission) I_{2D} as a function of (θ, φ) and the angle of the linearly polarized excitation field φ_{ex} is therefore

$$I_{2D} = I_0[\cos^2\theta + \sin^2\theta\cos^2(\varphi_{ex} - \varphi)]$$

For a single cycle of a polarization anisotropy measurement, the angle φ_{ex} is swept out over 2π radians (although the polar angle θ is not measured directly, it is calculated as discussed below). Figure 2A shows traces for two single CdSe−OPV nanostructures, which are averaged over 10π cycles of the pump polarization to mitigate fluorescence intermittency. M values are obtained by fitting to $a + b\cos^2\varphi$ (dashed lines in Figure 2A); from these M values, the orientation of the crystal c-axis is calculated as (see Appendix)

$$\theta = \sin^{-1}\sqrt{\frac{2M}{1+M}}$$

The resulting fits for the traces in Figure 2A yield $M = 0.58$, $\theta = 59°$ (black dot) and $M = 0.45$, $\theta = 52°$ (black square). By fitting these parameters, we can accurately determine the laboratory-frame orientation of the absorption moment of individual nanostructures.

We calculated analytically a normalized histogram of M values for randomly dispersed, perfectly degenerate 2D dipole QDs (see Appendix for details), resulting in a mean of value of modulation depths $\bar{M} = 0.4$ predicted for this system. In comparison, Figure 2B shows an experimental histogram of modulation depths for 200 single CdSe−OPV nanostructures with an average value $\bar{M}_{obs} = 0.47$, consistent with absorption from the nanocrystal core. This absorption behavior is attributed to the large mismatch in absorption cross sections between the CdSe nanocrystal ($\sim 5 \times 10^{-15}$ cm^2)[37] and OPV ligands (1×10^{-16} cm^2);[38] the absorption profile is dominated by the QD core at this wavelength. We note that fluorescence intermittency, which might manifest as an artificially large modulation depth, is effectively eliminated here by cyclic averaging, thus preventing blinking from dominating the measured M values.

Defocused Emission Patterns. In addition to probing dichroic PL intensity response with linearly polarized excitation, we sought to probe the nature of the emission moment and its correlation with the excitation directionality. For organic dyes such as Cy5 and DiIC$_{12}$, the absorption and emission moments have been shown to be nearly, but not completely, collinear.[16,36] Defocused imaging of spatial distributions of emitted photons through high numerical apertures has been used extensively to characterize single molecules[39,40] and quantum dots.[33−35] By introducing slight spherical aberration, anisotropies in the resulting images contain information on the transition dipole axis (or axes). This technique is useful because it allows for transition moment imaging while simultaneously monitoring photoluminescence dynamics. For single dye molecules, this method has been applied to determine rotational diffusion rates in porous media[41] and to verify modifications in radiative lifetime in relation to emitter orientation.[42] In single quantum dot studies, this technique has been applied to determine the orientation of the nanocrystal on the substrate surface. In this case, the image resulting from the 2D degenerate disk is the sum of two orthogonal linear dipoles (see Figure 3A), although groups have reported success in modeling experimental photon distributions using three linear dipoles[34] or a 2D + 1D scheme.[35]

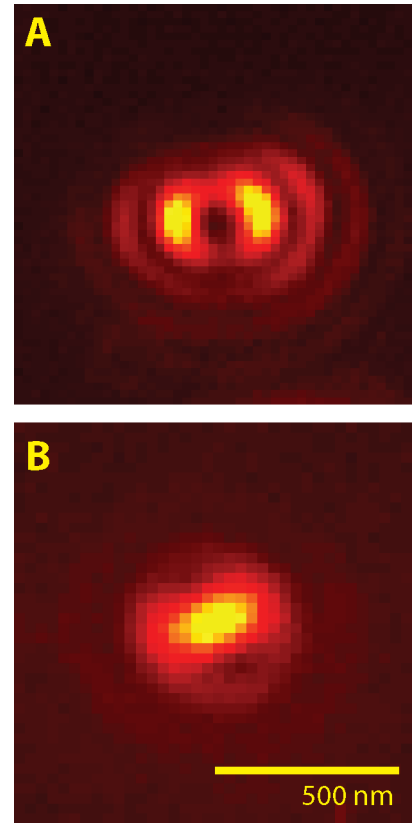

Figure 3. (A) Defocused image of ZnS-capped CdSe QD. The central node and side lobes are indicative of a 2D dipole with c-axis parallel to the sample plane. (B) Defocused emission pattern of CdSe−OPV, showing a distinct linear dipole emission pattern.

Unlike organic chromophores, where the emission dipole is typically fixed, the emission transition dipole of the nanocrystal core in a CdSe−OPV nanostructure displays complex behavior. Figure 3B shows a typical defocused emission pattern (DEP) from a single nanostructure with a fixed pump polarization characteristic of a linear transition dipole (dipole axis parallel to the major axis). All defocused images were spectrally filtered to exclusively collect emission from the CdSe core. During the linear dichroism runs, the DEP was observed to fluctuate as a function of the pump laser polarization for a significant fraction of the nanostructures imaged (reorientation of the major emission axis). As the samples were cast from THF onto neat glass and dried under dry N_2 flow, physical reorientation of the nanostructure throughout the course of the experiment is unlikely.

By combining linear dichroic and DEP measurements, we investigate the correlation between the absorption moment, emission moment, and excitation E

field for single nanostructures. Figure 4 shows simultaneous time trajectories of both the in-plane emission dipole orientation (A) and the PL intensity (C) from a single CdSe−OPV nanostructure under rotating pump polarization. The dashed line in panel C represents the rotating laser polarization, where the maxima (minima) correspond to V (H) polarization. The transition dipole orientations in panel A were determined by fits to the major axis of the DEP at a defocus depth $\delta z \approx 1000$ nm (toward the sample plane). Figure 4D shows the laboratory-frame phase-averaged emission from the trajectory in panel C along with a sine-squared fit (dashed line). Comparison to a histogram of laboratory-frame emission orientations over 100 s in Figure 4B shows two discrete linear emission orientations at roughly 45° and −50°, which correspond to the maximum and minimum absorption points in the phase-averaged emission curve. The discontinuous "jump" between two distinct orientations of the transition moment orientation was typical of the nanostructures displaying this behavior. The nanostructure shown in Figure 4 exhibits such a jump from −50° to +50° (with respect to the horizontal axis) between $t = 23$ and $t = 30$ s, after which it immediately returns to the previous mean value. As indicated in Figure 4, the jumps in emission orientation do not follow the laser polarization directly for the nanostructure, but rather "lag" the excitation field in time for 1−2 s. This was observed in almost all of the CdSe−OPV particles sampled.

Excitation Wavelength Dependence. To further verify the electronic interaction of surface ligands with the polarization properties of the CdSe core, we examined the linear dichroic and DEP behavior of CdSe−OPV using 514 nm excitation, where ligand absorption is negligible. While the absorption profiles of CdSe and the OPV ligands do not permit exclusive excitation of each moiety individually, excitation near the CdSe band edge completely avoids ligand excitation. In this way, the behavior of the hybrid system without ligand excitation is interrogated. Photoluminescence from single nanostructures was spectrally filtered to monitor QD emission strictly. At this wavelength, fluorescence intermittency becomes pronounced, providing further support for the role of photoexcited ligands in blinking suppression reported earlier.[26] The linear dichroism observed at 405 nm becomes less pronounced at 514 nm, and is complicated by the increased blinking at this wavelength. We make use of autocorrelation analysis to probe linear dichroism signatures that avoid these complications.

Figure 5 shows intensity trajectories $I(\theta)$ and corresponding autocorrelation functions $C(\gamma)$ for single CdSe−OPV nanoparticles illuminated at 405 nm (Figure 5A,B) and 514 nm (Figure 5C,D) over a 4π rotation of the excitation electric field. The dashed lines indicate the laboratory-frame electric vector in the $X-Y$ plane (maxima (minima) correspond to V(H) polarization). Autocorrelation analysis was performed to identify periodic fluorescence intensity peaks while simultaneously averaging over short dark periods. The linear polarization-dependent intensity autocorrelation functions are given by

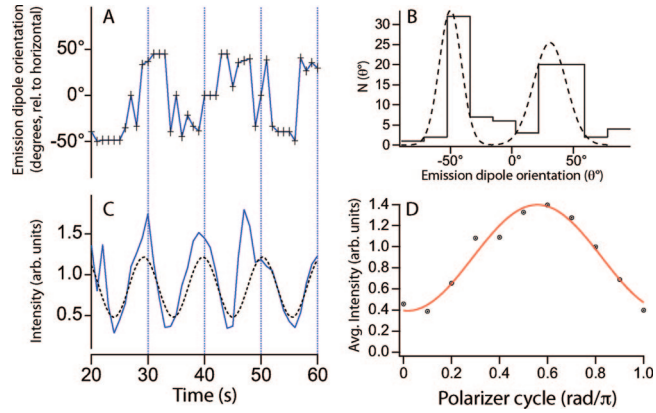

Figure 4. (A) Emission moment trajectory for a single CdSe−OPV under polarizer rotation (shown as dash in panel C) with respect to laboratory-frame horizontal axis. (B) Histogram of emission moment orientations for 100 s of collection. The Gaussian fits to the two features indicate an angle of 82° between $|X\rangle$ and $|Y\rangle$ axes. (C) Intensity trajectory for the same particle; the dashed line indicates the excitation polarization (see text). (D) Intensity for a single polarizer cycle averaged over 10 cycles (points), along with a $\cos^2 \varphi$ (solid line). Corresponding fitting parameters are $M = 0.57$, $\theta = 58°$.

$$C(\gamma) = \sum_{\theta} I(\theta)\, I(\theta + \gamma)$$

where $I(\theta)$ is the measured fluorescence intensity at a given electric field orientation, and γ is a stepped polarization offset. For linear absorbers with intensity maxima $I(\theta)_{max} \approx \cos^2 \theta$, this results in maxima in $C(\gamma)$ at intervals of π, which is clearly seen in Figure 5B under 405 nm excitation. The intensity trajectory in Figure 5A, taken using 100 ms integrations over 250 frames,

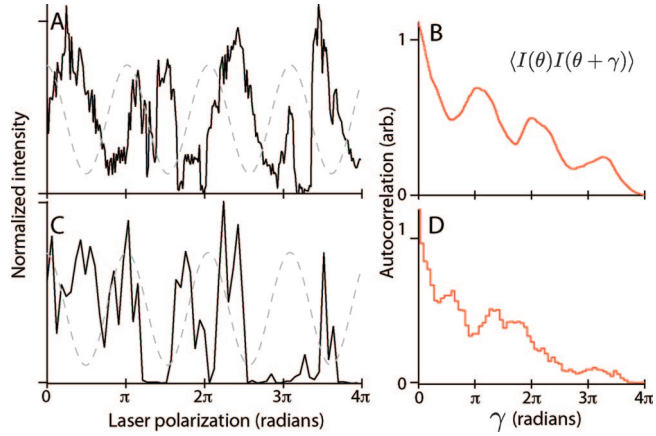

Figure 5. (A) Intensity trajectory (solid) as a function of laser polarization (dashed; maximum (minimum) corresponds to V(H) polarization) under 405 nm (ligand + QD) excitation. (B) Intensity autocorrelation $C(\gamma)$ for the trace in panel A, showing clear maxima at π intervals. (C) Intensity trajectory and laser polarization under 514 nm (QD only) excitation. (D) Corresponding autocorrelation analysis for the trajectory in panel C. The structure in $C(\gamma)$ arises from fluorescence bursts, with no features at π.

shows discrete fluorescence intermittency superimposed on a $\cos^2\theta$ polarization response. From this, the laboratory frame orientation of the absorption dipole moment can be obtained, although this information is not needed for these comparisons.

Both the intensity trajectories and autocorrelation functions for individual CdSe−OPV nanostructures showed distinct differences under 514 nm excitation compared with 405 nm. The intensity trajectory in Figure 5C consists of 65 1-s integrations over a 4π E field rotation. The fluorescence intensity required 10× binning due to the significantly lower absorption at this wavelength, characteristic of "bare" ZnS- or TOPO-capped CdSe QDs. The autocorrelation features are not present at π intervals, which indicates a lack of linear polarization response to the rotating field. The observed structure in $C(\gamma)$ arises from the fluorescence bursts and is not related to the polarization response. This was common for nearly all of the observed nanostructures.

To quantify the intermittency, we computed fluorescence duty factors (FDFs), which correspond to the percentage of the total experiment time a single nanostructure spends above a 2σ noise threshold ("on" state), at both 405 and 514 nm excitation wavelengths. Although these quantities have the disadvantage of being inherently dependent on both total experiment time and time binning δt, the suppressed blinking in these hybrid systems renders traditional "power law" blinking statistical analysis extremely difficult, hence motivating statistical analysis through both autocorrelation and FDFs. Histograms of these FDFs are shown in Figure 6. To accurately compare the two FDFs, data collected using 405 nm excitation were rebinned 10× from 100 ms up to 1 s. The dashed bars show the normalized histogram of FDFs from 160 CdSe-OPV nanostructures under 514 nm excitation, with an average value $\langle FDF\rangle_{514nm} = 0.60$. This largely unstructured distribution of FDFs is similar to that measured in this laboratory for ZnS-capped QDs.[26] The solid bars show the FDF distribution for 163 CdSe−OPV nanostructures excited at 405 nm (ligand + QD) with $\langle FDF\rangle_{405nm} = 0.74$. This measured distribution is strongly peaked near 1, indicating a large degree of blinking suppression at this wavelength.

It is clear from these data that the role of the photoexcited ligands is central to the observed modification in photophysical behavior for CdSe−OPV. Exciting the hybrid system to the red edge of the ligand absorption band results in fluorescence behavior similar to both CdSe/ZnS and CdSe-TOPO, including long excursions into dark states and largely degenerate 2D absorption behavior at thermal temperatures. By tuning to the tailing edge of the ligand absorption band, we gain access to a high degree of blinking suppression and highly linear absorption behavior. We believe the cause of this abrupt change in fluorescence properties at

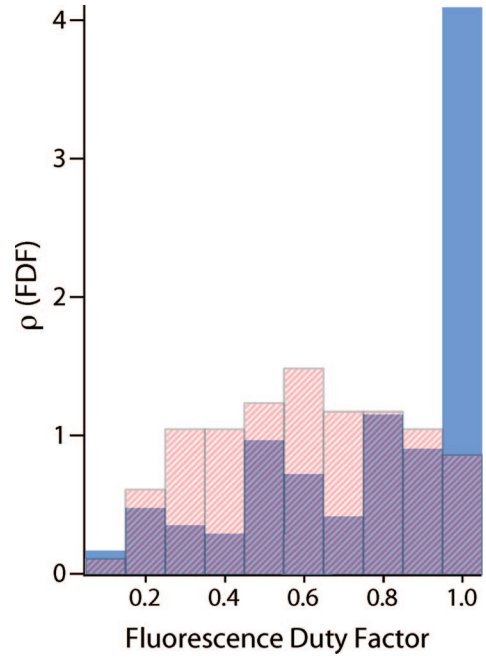

Figure 6. Histograms of fluorescence duty factors (fraction of time "on") under 405 nm (ligand + QD; solid bars) and 514 nm (QD only; dashed bars) excitation. The average computed FDFs were 0.74 (405 nm; sample size 163 nanostructures) and 0.60 (514 nm; 160 nanostructures).

these wavelengths arises from photoinduced charge separation in the surface-coordinated oligomers, which is only accessed at higher photon energies. These effects are discussed below.

DISCUSSION

The small (~3 meV) splitting observed between the $|X\rangle$ and $|Y\rangle$ states in CdSe/ZnS nanocrystals at cryogenic temperatures observed by Htoon et al.[23] is greatly enhanced by the presence of the OPV oligomers at the nanocrystal surface in the present experiments. The subset of ligands efficiently excited at a given pump polarization (proportional to $|E||\mu|\cos\theta$, with θ the angle between the pump polarization and oligomer transition moment μ) generates excitons in the organics localized near the nanocrystal surface. The difference in electronegativities between QD and semiconductor organic layer[43] drives electron transfer from ligand to QD across the saturated P−O linker, resulting in charge separated oligomers with a static charge distribution.

To get an estimate of the expected Stark shifts in CdSe−OPV, the electric field $E(r)$ in the nanocrystal interior due to a single charge separated oligomer was calculated as[44]

$$E(r) = \frac{3}{[\varepsilon_{NC}/\varepsilon_0 + 2]} \frac{q}{4\pi\varepsilon_0}\left[\frac{1}{r^2} - \frac{1}{(r+a)^2}\right]$$

where r is the distance from the nanocrystal surface, $\varepsilon_{NC}/\varepsilon_0$ is the ratio of dielectric constants of CdSe (taken to be 6 from Guyot-Sionnest et al.[45]) and free space, q is a unit charge, and α is the ligand length. The screen-

ing effect of the hole remaining localized on the ligand is included in the parameter α. This results in large internal fields near the coordinated ligand, which are on the order of 10^3 kV/cm at the nanocrystal interior. Comparison to bulk measurements by Empedocles et al.[46] shows that these field strengths are more than sufficient to cause Stark shifts on the order of 75−100 meV along the polarizable axis of the photoexcited ligand.

Pseudopotential calculations by Wang[47] on the effects of pinned charges near the QD surface support the above observations. The presence of a localized charge near the coordination site of the OPV ligand, generated by photoinduced charge separation when the organic excitation is efficiently driven, causes Coulombic separation of the internal QD electron and hole wave functions, and hence strong degeneracy breaking between $|X\rangle$ and $|Y\rangle$ states) along the axis defined by the conjugated ligand backbone. The rotation of the laser electric field in the $X-Y$ plane sequentially excites ligands with a large projection of their transition moments onto the laser electric vector, resulting in the fluctuation in emission moment described above. This effect is not as obvious in absorption, where intermittency and shot noise obscure secondary structure in the polarization anisotropy measurements.

CONCLUSION

We have studied the modified transition dipole moment characteristics of CdSe−OPV nanostructures using both polarization anisotropy and defocused widefield imaging techniques. These nanostructures exhibit the absorption characteristics of essentially 2D degenerate absorbers randomly distributed in a plane, albeit with a higher-than-expected average modulation depth ($\bar{M}_{obs} = 0.47$) compared to that predicted for an ideal, randomly distributed ensemble of 2D degenerate absorbers. However, the observed emission dipole transition obtained from widefield imaging appears as a fluctuating linear transition moment, which until now has not been observed in these so-called 2D degenerate systems. These effects are greatly diminished when the excitation wavelength is tuned away from the absorption band of the conjugated organic ligands coordinated to the QD surface. We attribute this effect to a large ligand-induced splitting of the orthogonal equatorial transition moment components. This splitting arises from a directional Stark shift from localized charges generated in the organic capping layer. This work presents an important first step toward the incorporation of single colloidal nanocrystal structures into device applications, where directionality in control is crucial.

METHODS

Details of synthetic procedures and characterization of CdSe−OPV nanostructures were reported previously.[48] Briefly, tri-*n*-octylphosphine-oxide (TOPO)-capped CdSe quantum dots of radius 2.1 nm were subjected to ligand exchange with OPV ligands consisting of 1.5 phenylene vinylene repeat units. The OPV ligands used show an absorption maximum ($\lambda_{max} = 355$ nm) superimposed on the typical CdSe absorption band structure (Figure 7). The composite nanostructures used in these experiments show a narrow photoluminescence emission spectrum at 580 nm (ca. 30−35 meV fwhm, Figure 7, inset) centered at the $1S_e-1S_{3/2}$ CdSe transition (see Figure 1 and Figure 2, inset). Particle diameters were measured by dynamic light scattering and AFM in tapping mode (Digital Instruments Bioscope) to confirm the presence of surface ligands, with average particle sizes of ~12 nm. For single molecule imaging and polarization measurements, CdSe−OPV nanostructures were cast from dilute THF solution onto plasma-cleaned glass coverslips, resulting in a mean square distance between particles of 4 μm^2. Imaging was performed on an inverted microscope (Nikon TE300) through a 1.4-NA 100× objective onto a 16-bit CCD camera (Princeton Instruments PhotonMax). A linearly polarized GaN laser (405 nm) was focused at the back aperture of the objective for widefield imaging of ~20 individual nanostructures in a single run; CW epi-illumination with a nominal excitation intensity of 2 W/cm^2 at the sample was used, resulting in excitation of both the CdSe nanocrystal and the OPV ligands. For excitation of only the QD core, a linearly polarized 514 nm Ar^+ laser line (Coherent Innova) was used at similar intensity. A combination of dichroic and long pass filters was employed to eliminate scattered laser light and to exclusively collect fluorescence from the CdSe core (580−30 band-pass). The filters were tested and showed a negligible polarization bias. For single molecule spectral measurements, fluorescence light was passed through a 430 nm long-pass filter to a calibrated spectrograph/CCD camera (Acton Spectrograph/Princeton Instruments Pixis).

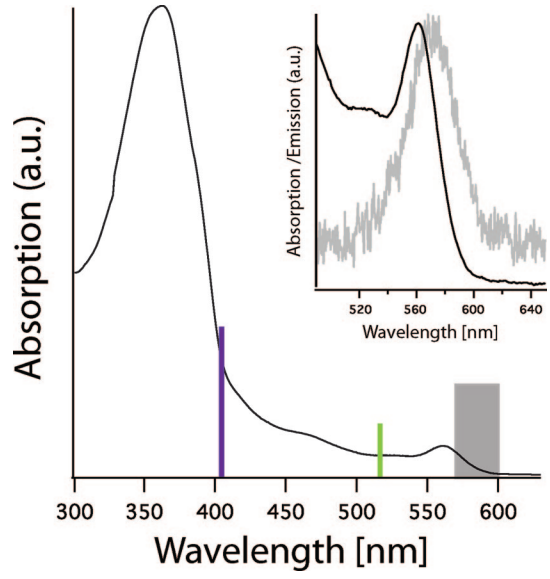

Figure 7. CdSe−OPV absorption spectrum showing OPV absorption ($\lambda_{max} = 355$ nm) and CdSe band-edge absorption in $CHCl_3$. The laser lines at 405 and 514 nm are shown by the vertical lines. Inset: Magnified band edge absorption (black) along with single CdSe-OPV emission spectrum (gray). For all experiments, only emission from the QD channel was collected (gray box; 580−30 band-pass).

For polarization anisotropy experiments, a computer-controlled broadband quartz half-wave (λ/2) retarder was used to rotate the polarization of the pump laser at a fixed angular frequency in the $X-Y$ sample plane at 0.1π rad/s (for emission moment tracking) and 0.04π rad/s (for modulation depth experi-

ments). For experiments requiring tracking of the polarization of the excitation laser in the laboratory-frame, the polarizer was synchronized with exposure times to extract phase information from the timing electronics. As a control for the polarization response experiments, 20 nm polystyrene spheres cast from semiconductor-grade methanol (FluoSpheres, Invitrogen Corporation) were subjected to excitation through the rotating polarizer, showing negligible polarization response.

Acknowledgment. We would like to acknowledge support from the NSF IGERT Program (DGE-0504485), the NSF-sponsored Center for Hierarchical Manufacturing at UMass Amherst (DMI-0531171), and the US DOE Basic Energy Sciences (05ER15965).

APPENDIX

We derived the expected probability density of modulation depths in an epi-illuminated sample of quantum dots, assuming (1) that the dots are completely spherical and have no preference of orientation and (2) that the transition moments of the dots are 2D degenerate in the plane perpendicular to the crystal *c*-axis of the nanocrystal. Again, we denote the orientation of the nanocrystal by the angular coordinates (θ, φ) made by the crystal *c*-axis relative to the *z*-axis (optic axis of the experiment, see inset of Fig. 2A). The intensity of excitation (and therefore of emission) I_{2d} as a function of (θ, φ) and the azimuthal angle of the linearly polarized excitation φ_{ex} is therefore

$$I_{2D} = I_0[\cos^2\theta + \sin^2\theta\cos^2(\varphi_{ex} - \varphi)]$$

In the course of a cycle of an anisotropy measurement, the angle φ_{ex} is swept out over 2π radians. The maximum and minimum intensity through the rotation will be

$$I_{max} = I_0 \qquad I_{min} = I_0\cos^2\theta$$

so that the modulation depth *M* becomes

$$M = \frac{I_{max} - I_{min}}{I_{max} + I_{min}} = \frac{\sin^2\theta}{2 - \sin^2\theta}$$

For a uniform orientation distribution θ of the nanocrystal *c*-axis, we can write the differential probability *P* over θ (and therefore over values of modulation depth) as

$$\frac{dP}{dM} \propto \frac{d\theta}{dM} = \frac{d}{dM}\left[\sin^{-1}\sqrt{\frac{2M}{1+M}}\right] = \frac{\sqrt{2}}{2}\frac{1}{\sqrt{1-M}}\left[\frac{1}{\sqrt{M+M^2}} - \frac{1}{1+M}\sqrt{\frac{M}{1+M}}\right]$$

Normalization gives

$$\int_0^1 \frac{d}{dM}\left[\sin^{-1}\sqrt{\frac{2M}{1+M}}\right]dM = \frac{\pi}{2}$$

so that we can write a normalized probability density over modulation depths as

$$\rho(M) = \frac{\sqrt{2}}{\pi}\frac{1}{\sqrt{1-M}}\left[\frac{1}{\sqrt{M+M^2}} - \frac{1}{1+M}\sqrt{\frac{M}{1+M}}\right]$$

Measurement of *M* for a nanostructure allows determination of the *c*-axis orientation by

$$\theta = \sin^{-1}\sqrt{\frac{2M}{1+M}}$$

REFERENCES AND NOTES

1. Kumar, S.; Scholes, G. D. Colloidal Nanocrystal Solar Cells. *Microchim. Acta* **2008**, *160*, 315–325.
2. Sun, B. Q.; Marx, E.; Greenham, N. C. Photovoltaic Devices Using Blends of Branched CdSe Nanoparticles and Conjugated Polymers. *Nano Lett.* **2003**, *3*, 961–963.
3. Blom, P. W. M.; deJong, M. J. M.; Vleggaar, J. J. M. Electron and Hole Transport in Poly(*p*-Phenylene Vinylene) Devices. *Appl. Phys. Lett.* **1996**, *68*, 3308–3310.
4. Greenham, N. C.; Peng, X. G.; Alivisatos, A. P. Charge Separation and Transport in Conjugated-Polymer/Semiconductor-Nanocrystal Composites Studied by Photoluminescence Quenching and Photoconductivity. *Phys. Rev. B* **1996**, *54*, 17628–17637.
5. Bussian, D.; Summers, M. A.; Iyer, P.; Liu, B.; Bazan, G. C.; Buratto, S. K. Single Molecule Spectroscopy of Tetrahedral Oligomeric Organic Semiconductors. *Abstr. Pap. Am. Chem. Soc.* **2004**, *227*, U545−U545.
6. Summers, M. A.; Kemper, P. R.; Bushnell, J. E.; Robinson, M. R.; Bazan, G. C.; Bowers, M. T.; Buratto, S. K. Conformation and Luminescence of Isolated Molecular Semiconductor Molecules. *J. Am. Chem. Soc.* **2003**, *125*, 5199–5203.
7. Buratto, S. K.; Summers, M. A.; Robinson, M. R.; Kemper, P. R.; Bushnell, J.; Bazan, G. C.; Bowers, M. T. Correlating Conformation and Luminescence in Single Oligophenylenevinylene Molecules. *Abstr. Pap. Am. Chem. Soc.* **2002**, *223*, C36−C36.
8. Premvardhan, L.; Peteanu, L. Electroabsorption Measurements and ab Initio Calculations of the Dipolar Properties of 2-(2 ′-Hydroxyphenyl)-Benzothiazole and -Benzoxazole: Two Photostabilizers That Undergo Excited-State Proton Transfer. *Chem. Phys. Lett.* **1998**, *296*, 521–529.
9. Peteanu, L.; Locknar, S. Stark Spectroscopy of an Excited-State Proton-Transfer Molecule: Comparison of Experimental and Computational Results for O-Hydroxyacetophenone. *Chem. Phys. Lett.* **1997**, *274*, 79–84.
10. Barbara, P. F.; Gesquiere, A. J.; Park, S. J.; Lee, Y. J. Single-Molecule Spectroscopy of Conjugated Polymers. *Acc. Chem. Res.* **2005**, *38*, 602–610.
11. Becker, K.; Da Como, E.; Feldmann, J.; Scheliga, F.; Csanyi, E. T.; Tretiak, S.; Lupton, J. M. How Chromophore Shape Determines the Spectroscopy of Phenylene-Vinylenes: Origin of Spectral Broadening in the Absence of Aggregation. *J. Phys. Chem. B* **2008**, *112*, 4859–4864.
12. Da Como, E.; Becker, K.; Feldmann, J.; Lupton, J. M. How Strain Controls Electronic Linewidth in Single Beta-Phase Polyfluorene Nanowires. *Nano Lett.* **2007**, *7*, 2993–2998.
13. Voigt, M.; Langner, A.; Schouwink, P.; Lupton, J. M.; Mahrt, R. F.; Sokolowski, M. Picosecond Time Resolved Photoluminescence Spectroscopy of a Tetracene Film on Highly Oriented Pyrolytic Graphite: Dynamical Relaxation, Trap Emission, and Superradiance. *J. Chem. Phys.* **2007**, *127*, 114705.
14. Soujon, D.; Becker, K.; Rogach, A. L.; Feldmann, J.; Weller, H.; Talapin, D. V.; Lupton, J. M. Time-Resolved Forster Energy Transfer from Individual Semiconductor Nanoantennae to Single Dye Molecules. *J. Phys. Chem. C* **2007**, *111*, 11511–11515.
15. Ha, T.; Enderle, T.; Chemla, D. S.; Selvin, P. R.; Weiss, S. Single Molecule Dynamics Studied by Polarization Modulation. *Phys. Rev. Lett.* **1996**, *77*, 3979–3982.
16. Macklin, J. J.; Trautman, J. K.; Harris, T. D.; Brus, L. E. Imaging and Time-Resolved Spectroscopy of Single Molecules at an Interface. *Science* **1996**, *272*, 255–258.
17. Kumar, P.; Lee, T. H.; Mehta, A.; Sumpter, B. G.; Dickson, R. M.; Barnes, M. D. Photon Antibunching from Oriented Semiconducting Polymer Nanostructures. *J. Am. Chem. Soc.* **2004**, *126*, 3376–3377.
18. Lee, T. H.; Kumar, P.; Mehta, A.; Xu, K. W.; Dickson, R. M.; Barnes, M. D. Oriented Semiconducting Polymer Nanostructures as on-Demand Room-Temperature Single-Photon Sources. *Appl. Phys. Lett.* **2004**, *85*, 100–102.

19. Mehta, A.; Kumar, P.; Dadmun, M. D.; Zheng, J.; Dickson, R. M.; Thundat, T.; Sumpter, B. G.; Barnes, M. D. Oriented Nanostructures from Single Molecules of a Semiconducting Polymer: Polarization Evidence for Highly Aligned Intramolecular Geometries. *Nano Lett.* **2003**, *3*, 603–607.
20. Kumar, P.; Mehta, A.; Dadmun, M. D.; Zheng, J.; Peyser, L.; Bartko, A. P.; Dickson, R. M.; Thundat, T.; Sumpter, B. G.; Noid, D. W.; Barnes, M. D. Narrow-Bandwidth Spontaneous Luminescence from Oriented Semiconducting Polymer Nanostructures. *J. Phys. Chem. B* **2003**, *107*, 6252–6257.
21. Efros, A. L. Luminescence Polarization of CdSe Microcrystals. *Phys. Rev. B* **1992**, *46*, 7448–7458.
22. Efros, A. L.; Rodina, A. V. Band-Edge Absorption and Luminescence of Nonspherical Nanometer-Size Crystals. *Phys. Rev. B* **1993**, *47*, 10005–10007.
23. Htoon, H.; Furis, M.; Crooker, S. A.; Jeong, S.; Klimov, V. I. Linearly Polarized 'Fine Structure' of the Bright Exciton State in Individual CdSe Nanocrystal Quantum Dots. *Phys. Rev. B* **2008**, *77*, 035328.
24. Montiel, D.; Yang, H. Observation of Correlated Emission Intensity and Polarization Fluctuations in Single CdSe/ZnS Quantum Dots. *J. Phys. Chem. A* **2008**, *112*, 9352–9355.
25. Hu, J. T.; Li, L. S.; Yang, W. D.; Manna, L.; Wang, L. W.; Alivisatos, A. P. Linearly Polarized Emission from Colloidal Semiconductor Quantum Rods. *Science* **2001**, *292*, 2060–2063.
26. Hammer, N. I.; Early, K. T.; Sill, K.; Odoi, M. Y.; Emrick, T.; Barnes, M. D. Coverage-Mediated Suppression of Blinking in Solid State Quantum Dot Conjugated Organic Composite Nanostructures. *J. Phys. Chem. B* **2006**, *110*, 14167–14171.
27. Efros, A. L.; Rosen, M.; Kuno, M.; Nirmal, M.; Norris, D. J.; Bawendi, M. Band-Edge Exciton in Quantum Dots of Semiconductors with a Degenerate Valence Band: Dark and Bright Exciton States. *Phys. Rev. B* **1996**, *54*, 4843–4856.
28. Empedocles, S. A.; Norris, D. J.; Bawendi, M. G. Photoluminescence Spectroscopy of Single Cdse Nanocrystallite Quantum Dots. *Phys. Rev. Lett.* **1996**, *77*, 3873–3876.
29. Nirmal, M.; Norris, D. J.; Kuno, M.; Bawendi, M. G.; Efros, A. L.; Rosen, M. Observation of the Dark Exciton in CdSe Quantum Dots. *Phys. Rev. Lett.* **1995**, *75*, 3728–3731.
30. Chung, I. H.; Shimizu, K. T.; Bawendi, M. G. Room Temperature Measurements of the 3d Orientation of Single CdSe Quantum Dots Using Polarization Microscopy. *Proc. Natl. Acad. Sci. U.S.A.* **2003**, *100*, 405–408.
31. Empedocles, S. A.; Neuhauser, R.; Bawendi, M. G. Three-Dimensional Orientation Measurements of Symmetric Single Chromophores Using Polarization Microscopy. *Nature* **1999**, *399*, 126–130.
32. Bohmer, M.; Enderlein, J. Orientation Imaging of Single Molecules by Wide-Field Epifluorescence Microscopy. *J. Opt. Soc. Am., B* **2003**, *20*, 554–559.
33. Brokmann, X.; Coolen, L.; Hermier, J. P.; Dahan, M. Emission Properties of Single CdSe/ZnS Quantum Dots Close to a Dielectric Interface. *Chem. Phys.* **2005**, *318*, 91–98.
34. Patra, D.; Gregor, I.; Enderlein, J.; Sauer, M. Defocused Imaging of Quantum-Dot Angular Distribution of Radiation. *Appl. Phys. Lett.* **2005**, *87*, 101103.
35. Schuster, R.; Barth, M.; Gruber, A.; Cichos, F. Defocused Wide Field Fluorescence Imaging of Single CdSe/ZnS Quantum Dots. *Chem. Phys. Lett.* **2005**, *413*, 280–283.
36. Ha, T.; Laurence, T. A.; Chemla, D. S.; Weiss, S. Polarization Spectroscopy of Single Fluorescent Molecules. *J. Phys. Chem. B* **1999**, *103*, 6839–6850.
37. Leatherdale, C. A.; Woo, W. K.; Mikulec, F. V.; Bawendi, M. G. On the Absorption Cross Section of CdSe Nanocrystal Quantum Dots. *J. Phys. Chem. B* **2002**, *106*, 7619–7622.
38. Sierra, C. A.; Lahti, P. M. A Photolumineseent, Segmented Oligo-Polyphenylenevinylene Copolymer with Hydrogen-Bonding Pendant Chains. *Chem. Mater.* **2004**, *16*, 55–61.
39. Bartko, A. P.; Dickson, R. M. Imaging Three-Dimensional Single Molecule Orientations. *J. Phys. Chem. B* **1999**, *103*, 11237–11241.
40. Dickson, R. M.; Norris, D. J.; Moerner, W. E. Simultaneous Imaging of Individual Molecules Aligned Both Parallel and Perpendicular to the Optic Axis. *Phys. Rev. Lett.* **1998**, *81*, 5322–5325.
41. Dickson, R. M.; Norris, D. J.; Tzeng, Y. L.; Moerner, W. E. Three-Dimensional Imaging of Single Molecules Solvated in Pores of Poly(Acrylamide) Gels. *Science* **1996**, *274*, 966–969.
42. Brokmann, X.; Coolen, L.; Dahan, M.; Hermier, J. P. Measurement of the Radiative and Nonradiative Decay Rates of Single CdSe Nanocrystals through a Controlled Modification of Their Spontaneous Emission. *Phys. Rev. Lett.* **2004**, *93*, 107403.
43. Ginger, D. S.; Greenham, N. C. Photoinduced Electron Transfer from Conjugated Polymers to Cdse Nanocrystals. *Phys. Rev. B* **1999**, *59*, 10622–10629.
44. Jackson, J. D., *Classical Electrodynamics*, 3rd ed.; Wiley: New York, 1999; p xxi.
45. Guyot-Sionnest, P.; Wehrenberg, B.; Yu, D. Intraband Relaxation in CdSe Nanocrystals and the Strong Influence of the Surface Ligands. *J. Chem. Phys.* **2005**, *123*, 074709.
46. Empedocles, S. A.; Bawendi, M. G. Quantum-Confined Stark Effect in Single CdSe Nanocrystallite Quantum Dots. *Science* **1997**, *278*, 2114–2117.
47. Wang, L. W. Calculating the Influence of External Charges on the Photoluminescence of a CdSe Quantum Dot. *J. Phys. Chem. B* **2001**, *105*, 2360–2364.
48. Sudeep, P. K.; Early, K. T.; McCarthy, K. D.; Odoi, M. Y.; Barnes, M. D.; Emrick, T. Monodisperse Oligo(Phenylene Vinylene) Ligands on CdSe Quantum Dots: Synthesis and Polarization Anisotropy Measurements. *J. Am. Chem. Soc.* **2008**, *130*, 2384–2385.